Seismic Behavior of High-rise Steel Moment-resisting Frames with Vertical Mass Irregularity

수직질량 비정형이 존재하는 고층 강 모멘트-저항골조의 지진 거동

최 병 정* 송 인 환**
Byong Jeong Choi Song, In-Hawn

국문요약

고층의 강 모멘트저항골조에 대한 지진 응답을 살펴보기 위해서 동적해석을 실시하였다. 구조물은 세가지의 다른 설계절차로 의도적으로 설계하였고 그 세가지의 개념은 강도 지배설계, 강기둥-약보 지배설계, 횡변위 지배설계이다. 그렇게 설계한 구조물이 각각 질량비정형이 존재하도록 하여 횡변위, 소성힌지, 이력에너지 입력 및 요구응력에 대해서 토론하였다. 미래에 설계에의 응용을 위해서 최대 지반가속도로 표현한 두 등급의 지진 하중을 이용해서 이력에너지 입력요구 곡선을 제시하였다.

주요어 : 질량비정형, 이력에너지입력, 횡변위지배설계, 지진응답

ABSTRACT

Dynamic analyses were carried out to study the seismic response of high-rise steel moment-resisting frames in sixteen story buildings. The frames are intentionally designed by three different design procedures; strength controlled design, strong column-weak beam controlled design, and drift controlled design. The seismic performances of the so-designed frames with vertical mass irregularities were discussed in view of drift ratio, plastic hinge rotation, hysteretic energy input and stress demand. A demand curve of hysteretic energy inputs was also presented with two earthquake levels in peak ground accelerations for a future design application.

Key words : mass irregularity, hysteretic energy input, drift controlled design, seismic response

1. Introduction

This research was carried out to investigate the hysteretic energy input characteristics, plastic rotation distributions, and story drift ratios on sixteen story high-rise steel moment resisting frames. The paper covered on the mass and stiffness irregularities using 16-story steel moment-resisting frames.

Nowadays in many countries many buildings are constructed to fulfill functions for both commercial and residential purposes. The lower stories of the building are normally used for the commercial purposes, say below the third story, and the rest of upper stories would be used for the residential purpose. These types of buildings are one of attractive building types because they can fulfill many functions in one building. The major functions of these buildings are housing, shopping, commerce, parking, dining, and so on.

There exist mass irregularities in this type of buildings. The structural safety of this type of building is easily overlooked without checking dynamic analysis under strong earthquake ground motions. Seismic responses, especially energy characteristics, are not fully researched using structures with vertical mass irregularities. It is interesting to investigate the irregular mass and strength difference effects, including loading path, hysteretic energy input characteristics, plastic rotation, drift ratios and detailed stress distributions, for these types of structures subjected to the various seismic loadings. For this type of buildings it is necessary to install very large transfer-girders in the lower floors. Then, the transfer-girder should carry the upper floor's loadings to the columns at the lower stories. Under earthquake loading, the structural system of the mentioned buildings can be damaged due to the irregularity of the stiffness or mass. In other words, the stiffness or vertical mass irregularity can occur in this type of building. The stiffness and mass irregularities can happen unknowingly in any design phases if engineers forget to check the mass or stiffness irregularities according to the Uniform Building Code.[1] This point is the most critical problem in engineering practice.

Therefore, this paper considers the seismic response of the steel moment resisting frames through examining the vertical mass irregularities under various seismic loadings. The seismic response results in terms of the hysteretic energy inputs, plastic rotations, and story drifts using sixteen story steel moment resisting frames are presented. The stress

* 정회원 · 경기대학교 건축전문대학원 조교수, 공학박사
(대표저자 : bjchoi@kuic.kyonggi.ac.kr)
** 학생회원 · 경기대학교 건축공학과 대학원, 공학석사
본 논문에 대한 토의를 2004년 4월 30일까지 학회로 보내 주시면 그 결과를 게재하겠습니다. (논문접수일 : 2003. 7. 29 / 심사종료일 : 2004. 1. 18)

distribution at the beam-column connection of the first floor was studied to take account for the damage patterns under the same seismic loading using the finite element analysis. Finally, the amount of hysteretic energy input at the two design levels of earthquake ground motions in quantitative manner are considered.

2. Background

A structure is considered to be irregular if it has significant physical discontinuities in its configuration or in its lateral-force resisting system. Many structural codes specify limited values for structural irregularities. According to the 1997 UBC[1], the following irregularities exist.

Mass irregularity: Mass(weight) irregularity is considered to exist where the effective mass of any story is more than 150% of the effective mass of an adjacent story. A roof that is lighter than the floor below need not be considered.

Stiffness irregularity : A soft story is one in which the lateral stiffness is less than 70% of that of the story above, or less than 80% of the average stiffness of the next three stories above.

Discontinuity in capacity(weak story) : A weak story is one in which the story strength is less than 80% of that of the story above. The story strength is the total strength of all seismic-resisting elements that share the story shear for the direction under consideration.

The irregularities can occur as setbacks, mass irregularities, stiffness irregularities, or weak stories. The vertical irregularities in a building may result in a concentration of forces of deflections or in an undesirable load path in the vertical lateral-force-resisting system. In the extreme cases, this can result in serious damage to or collapse of a building, since the lateral system is often integral with the gravity-load-resisting system.[2] To date, the detailed evaluations of the vertical irregularities for tall steel moment resisting frames are not fully carried out on hysteretic energy inputs, plastic rotations, drift ratios, and stress demands. These research points are also easily overlooked in many undeveloped countries.

The hysteretic energy input is a very valuable parameter for investigating the seismic response of steel moment resisting frames subjected to various seismic loadings. The displacement ductility itself does not fully demonstrate the damage pattern of the structure. However, the hysteretic energy input represents the low cycle fatigue and structural damage. Accordingly, the hysteretic energy input parameter was used as one of the main parameters in this essay. Uang and Bertero[3], Kuwamura and Galambos[4], and Akiyama[5] measured the energy input of structures due to various earthquake ground motions. These investigations proved the possibility that the hysteretic energy input is a good parameter for explaining structural demands and damages. Valmundsson et al.[6] published a paper regarding seismic response of building frames with vertical irregularities. Their paper mainly focused on the ductility demand ratio using multi-degree of freedom(MDOF) systems. However, the hysteretic energy input characteristics and plastic rotations of the MDOF systems with vertical irregularities were not fully covered in their research.

Therefore, it is necessary to study the seismic responses of the vertical irregularities using various parameters. This proposed research was performed to find the hysteretic energy input characteristics, plastic rotations, drift ratios, and stress distribution pattern of sixteen story steel moment resisting frames with vertical mass irregularities. The seismic responses of the above parameters are examined to find the critical damage patterns of mass irregularities using the time history analysis and the finite element method. The additional study using the finite element analysis was very beneficial for understanding the stress demand at the beam-column connection area with vertical mass irregularities.

3. Hysteretic Energy Input

There are many indices for damage evaluation of structures subjected to earthquake ground motions. The hysteretic energy input damage index is especially important. When a building is subjected to earthquakes, a structure may go through nonlinear cyclic responses. The cyclic responses can be represented by hysteretic energy. The various energy terms can be defined by integrating the equation of motion of an inelastic system. The governing equation[7] for an inelastic system is as follows :

$$m\ddot{u}_c + \dot{u} + f_S(u, u) = -m\ddot{u}_g(t) \tag{1}$$

$$\int_0^u m\ddot{u}(t)du + \int_0^u c\dot{u}(t)du + \int_0^u f_S(u, \dot{u})du = -\int_0^u m\ddot{u}_g(t)du \tag{2}$$

The energy dissipated by hysteretic yielding is

$$E_h(t) = \int_0^u f_S(u, \dot{u})du - E_S(t) \tag{3}$$

Eventually, the energy should be balanced to keep the stability of the system.

$$E_I(t) = E_K(t) + E_D(t) + E_S(t) + E_h(t) \quad (4)$$

Eq. (4) implies that total energy equals the sum of damping energy(E_D), kinetic energy(E_K), strain energy(E_S) and hysteretic (E_h). The hysteretic energy demand on the lateral-load resisting elements was further characterized by a factor similar to the displacement ductility demand.

$$\mu_h = \frac{u_{\max}}{u_y} = \frac{E_h}{f_y u_y} + 1 \quad (5)$$

$$E_h = f_y(u_{\max} - u_y) \quad (6)$$

The hysteretic energy ductility demand was defined as one plus total hysteretic energy dissipated by the element during all inelastic cycles divided by twice the energy absorbed at the first yield shown in Fig. 1.[8] Accordingly, in a monotonic loading condition hysteretic energy demand can be acquired as represented in equation six.

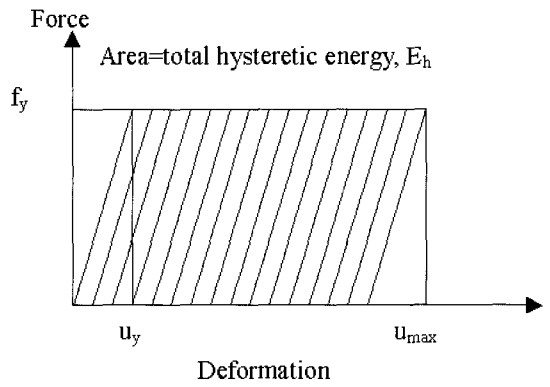

Fig. 1 Definition of hysteretic energy ductility demand

On the other hand energy input can be expressed by total energy input divided by the mass of a system. Uang et al. measured the absolute energy input using a six story braced steel frame.[9] While the relative energy formulation has been used in the majority of the previous investigation, their study shows that the absolute energy equation is physically more meaningful. They presented a formula of energy input for the SDOF system as follows.

$$\frac{E_i^{\max}}{m} = 0.5(1.0 + 1.0t_D)^2 \dot{u}_{go}^2 \quad (7)$$

Fajfar et al.[10] proposed the maximum input energy, which is imparted to systems with fundamental periods in the vicinity of the predominant period of the ground motion. They proposed the equation of energy input that can be written in the form as :

$$\frac{E_I}{m} = 0.85 \frac{v_g}{a_g} \int \ddot{u}_g^2 dt \quad (8)$$

As we studied, all the energy equation was explained in the form of total energy input divided by mass. However, it is also meaningful to explain energy by using the total hysteretic energy input of the represented structural damage. The energy characteristics were plotted in the form of the total hysteretic energy input divided by the structure mass to plot an energy demand curve for the future.

4. Modelling

4.1 Selection of earthquake level

To examine the characteristics of selected earthquake ground motions, the response spectrum analyses were carried out using SPCEQ program.[11] Two design earthquake levels(DEQL) scaled to 0.3g(DEQL I) and 0.6g(DEQL II) were used in this study. Three earthquake ground motions were used and scaled to the two design earthquake levels. The characteristics of the ground motions were as shown in Table 1. The normalized response spectrums of earthquake ground motions are shown in Figs. 2.

4.2 Loading Plan

To perform the nonlinear time history analysis, the DRAIN2D+ program[12] was used. The Strand7[13] is also used to evaluate the detailed stress response at the exterior beam-column connection of the first floor for a sixteen story steel moment resisting frame. No rigid zone was

Table 1 Characteristics of earthquake ground motions

No.	Ground Motion	Component	Epicentral distance, km	A/g	$\dot{u}_{go}$, cm-s-1	t_g, sec.	t_D, sec.	Geology
EQ 1	El Centro May 18, 1940	S00E	14.9	0.3489	33.45	0.55	24.46	Stiff Soil
EQ 2	Miyagi June 12, 1978	EW	160	0.2073	25.27	1.12	24.78	Alluvium
EQ 3	Northridge Jan. 17, 1994	New-360	30.72	0.5963	56.89	0.68	5.50	Alluvium

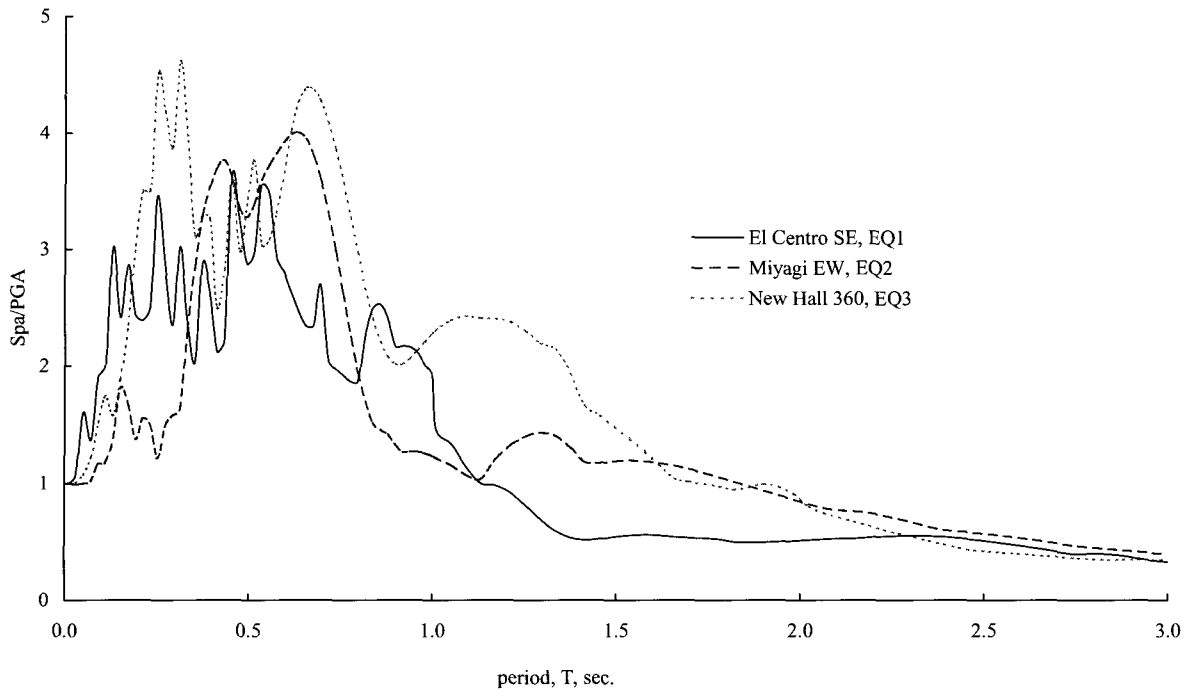

Fig. 2 Normalized acceleration response spectrum with 2% damping ratio

considered or beam-column element was used in the DRAIN+ program.

The two nominal strengths of beam and column were assumed to be 2.4 and 2.8tf/cm^2, respectively. Loads are applied to three major floors: the roof, the middle level floors, and the ground floor, respectively. For the roof, dead and live loads were 350 and 200kgf/m^2, respectively. For middle level floors, dead load and live load were 500 and 200kgf/m^2, respectively. For the ground floor, dead load and live load were 540 and 500kgf/m^2, respectively. The 25% of live loads were used in the nonlinear time-history analyses.

Relative energy was used to define work of an equivalent force(mass multiplied by the ground acceleration) on the fixed-based system. The rigid body translation on the structure was not considered in the study.

Damping is another factor affecting hysteretic energy.[14],[15] For simplicity, the viscous damping was fixed at 2%. Straining hardening of 2% was assumed for the MDOF systems. The hysteretic energy input was investigated to find the hysteretic energy input pattern of the steel moment resisting frames with vertical mass irregularities. The natural periods and mode shapes of DRFT-C frame were shown in Fig. 5. It seems that the natural periods of the studied frames are little high. The main reasons of high natural periods were contributed by the mass increment and high seismic coefficients ranged from 0.4 to 0.45 in the targeted model. To account the condition, the Rayleigh damping was used in the analyses.

4.3 Design and analysis of steel moment resisting frames

The overall design schedule is shown in Table 2. Steel moment-resisting frames in sixteen-story building were designed by different design concepts. The three design philosophies, or basic systems were called strength design (SD-C), strong-column/weak-beam design(SCWB-C), and drift control design(DRFT-C). The following two equations can be used for SCWB condition analysis at any beam-to-column connection. Eq. (9)[16] was used for studying these three designs.

$$\frac{\Sigma Z_c(F_{yc}-P_{uc}/A_g)}{\Sigma Z_b F_{yb}} \geq 1.0 \tag{9}$$

$$\frac{\Sigma Z_c(F_{yc}-P_{uc}/A_g)}{V_n d_b H/(H-d_b)} \geq 1.0 \tag{10}$$

where,

A_g : Gross area of a column
F_{yb} : Specified minimum yield strength of a beam
F_{yc} : Specified minimum yield strength of a column
H : Average of the story heights above and below the joint
P_{uc} : Required axial strength in the column(in compression)
V_n : Nominal strength of the panel zone
Z_b : Plastic section modulus of a beam
Z_c : Plastic section modulus of column
d_b : average overall depth of beams framing into the connection

The plastic section modulus of all column members were

Table 2 Beam/column schedules with H-shaped members for control systems, mm

Story level	SD system		SCWB system		DRFT system	
	Beam	Int. Cols. Ext. Cols.	Beam	Int. Cols. Ext. Cols.	Beam	Int. Cols. Ext. Cols.
1-2	582×300×12×17	792×300×14×22 800×300×14×26	582×300×12×17	792×300×14×22 792×300×14×22	582×300×12×17	792×300×14×22 792×300×14×22
3-4	582×300×12×17	588×300×12×20 582×300×12×17	582×300×12×17	692×300×13×20 582×300×12×17	582×300×12×17	692×300×13×20 582×300×12×17
5-6	582×300×12×17	588×300×12×20 482×300×11×15	582×300×12×17	588×300×12×20 482×300×11×15	582×300×12×17	588×300×12×20 582×300 12×17
7-8	582×300×12×17	488×300×11×18 390×300×10×16	582×300×12×17	588×300×12×20 482×300×11×15	582×300×12×17	588×300×12×20 488×300×11×18
9-10	582×300×12×17	482×300×11×15 386×299× 9×14	582×300×12×17	582×300×12×17 386×299× 9×14	582×300×12×17	588×300×12×20 488×300×11×18
11-12	488×300×11×18	386×299× 9×14 340×250× 9×14	488×300×11×18	482×300×11×15 340×250× 9×14	488×300×11×18	588×300×12×20 386×299× 9×14
13-14	482×300×11×15	340×250× 9×14 294×200× 8×12	482×300×11×15	434×299×10×15 340×250× 9×14	482×300×11×15	482×300×11×15 340×250× 9×14
15-16	506×201×11×19	200×200× 9×12 200×200× 8×12	506×201×11×19	434×299×10×15 340×250× 9×14	506×201×11×19	482×300×11×15 340×250× 9×14

not reduced in the design procedure.

The SCWB-C frame does not follow the drift limit by the code of Eq. (7). The drift limit of 0.015h was observed in the DRFT-C frame. The LRFD method and 1997 UBC code were used for those designs. To get smoothed design strength over the floor, all designs were made in a way that the interaction of flexure and axial compression to each beam-column connection ranged between 0.85 and 0.95 that are surely smaller than 1.0. The plan view of the steel moment resisting frame is shown in Fig. 3.

After the design of the three basic systems, the mass of the basic system is artificially changed to create mass irregularities without changing the total mass shown in Fig. 4. With Case 1, the mass at the ground floor was increased by 50% point and the mass at the second-floor was decreased by 50% for three basic designs. Therefore, the vertical mass irregularity of 200% was made in an adjacent story. The value of mass(m) by 3.5469tf-s^2/cm was used in the design.

The same adjustments were made for cases 2 and 3 to the eight-floor and fifteen-floor, respectively with the three

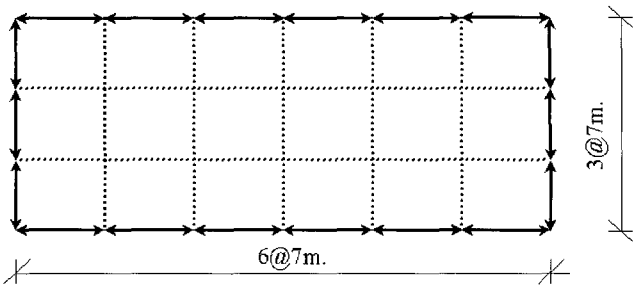

Fig. 3 Plan view of the steel moment perimeter frame

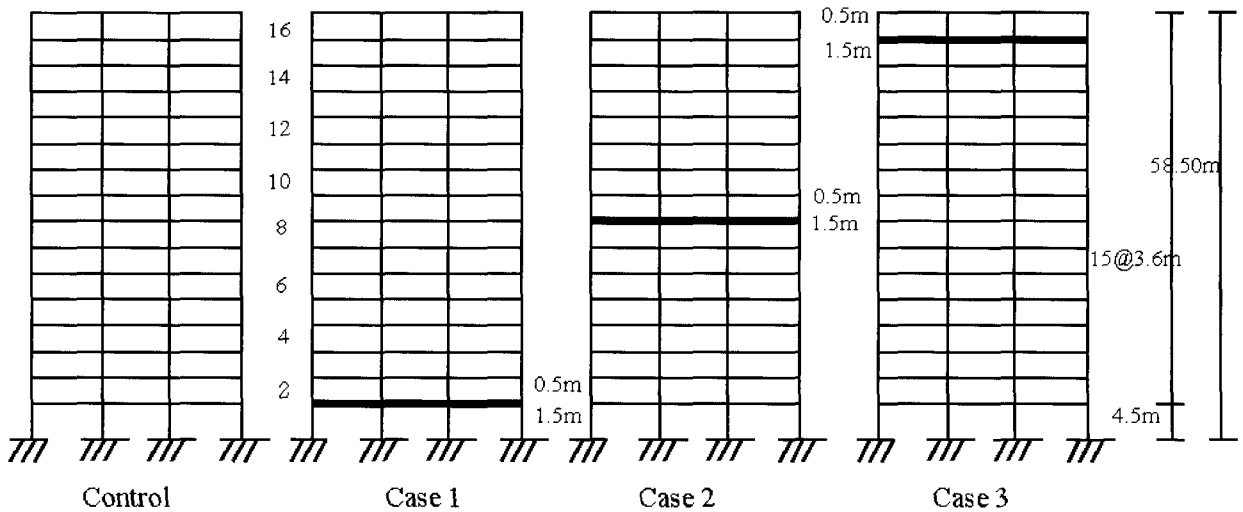

Fig. 4 Mass variation schedules for 16-story structures

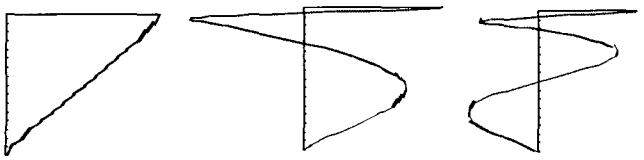

T_1=4.47 T_2=1.61 T_3=0.94

ϕ_{161}=0.96 ϕ_{162}=0.93 ϕ_{163}=0.83

Fig. 5 Mode shapes for DRFT-C Frame in 16-story

basic systems. However, the total structural mass has not been changed in each case to keep the structural integrity. The selected member sizes of the SD, SCWB and DRFT systems are shown in Table 2.

The overall analysis was carried out by the following :

(1) The nonlinear push over analysis was carried out for the three basic systems.
(2) The nonlinear time history analysis was performed to evaluate the seismic response including hysteretic energy input, plastic rotation, and drift for the SD system.
(3) Next, the procedure (2) was performed for cases 1, 2, and 3 of the SD system.
(4) The procedures (1), (2), and (3) were repeatedly performed for SCWB and DRFT systems.
(5) Finally, finite element analysis was performed for DRFT system where the 2D plate element was used.

5. Results And Discussions

5.1 Nonlinear pushover analysis

The nonlinear pushover analysis was performed to find out any deterioration of the basic systems. The member size can be increased if any strength degradation is found from the pushover analysis. The pushover analysis results are shown in Fig. 6. The strength and stiffness of SCWB-C and DRFT-C systems were very similar to the SD system. The DRFT-C(drift control) system showed the highest strength among them. The SD-C system showed the least yield strength. Accordingly, Fig. 6 clearly showed the stiffness and strength irregularity. However, displacements at the point of yield strength for the three systems were quite close in the nonlinear pushover analysis.

The nonlinear pushover and cyclic loading results showed that the three basic systems are stable. Therefore, further analysis for the three systems was continued without increase.

5.2 Strength and stiffness irregularity of the three control systems

The primary objective of this section is to study strength and stiffness of seismic response of steel moment resisting frames. The strength and stiffness effects were studied in view of drift ratio and plastic rotation for normal frames.

The difference of the stiffness and yield strength ratio of the three systems, SD-C, SCWB-C and DRFT-C frames are 1: 1.18: 1.32, respectively. In other words, the yield strength of the DRFT control model(DRFT-C) is 1.32 times higher than the SD control frame(SD-C).

As shown in Fig. 7 through Fig. 10 the drift ratio was evaluated with three earthquakes. The results are shown with EQ1 and EQ2 in peak ground accelerations scaled to 0.3g and 0.6g. In case of SD-C frame, the drift ratio resulted

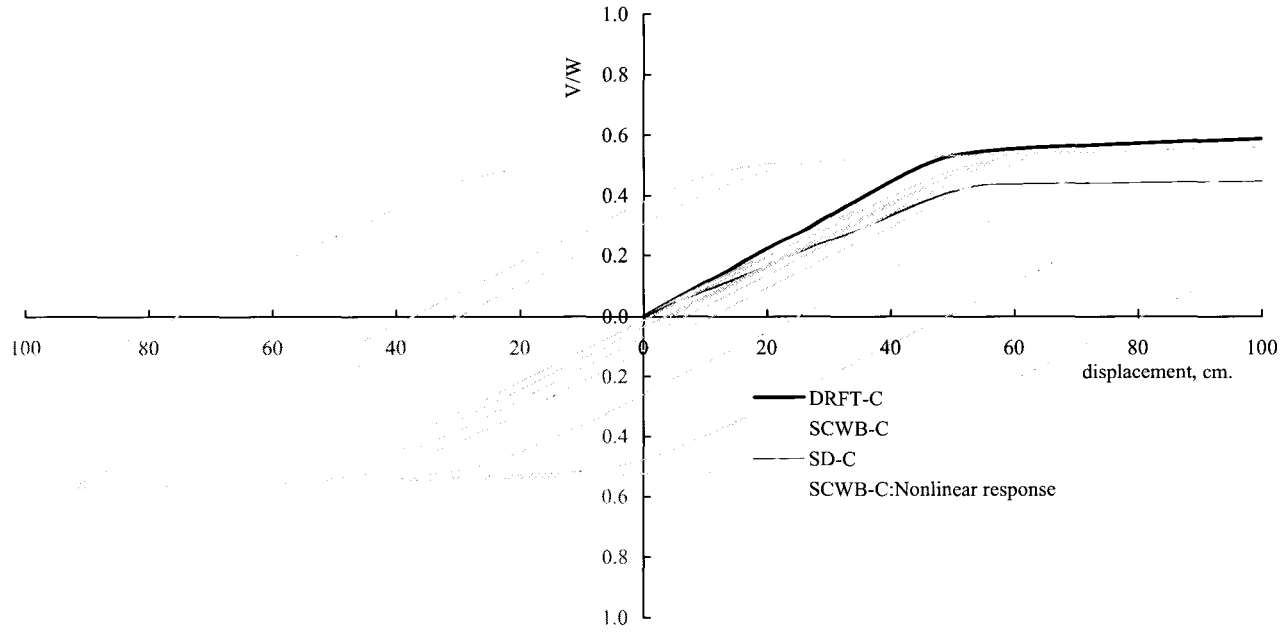

Fig. 6 Roof displacements of three steel moment resisting frames for control frames

in high values compared with SCWB-C and DRFT-C frames at upper floors around the twelfth story through the sixteenth story shown in Fig. 7. In case of EQ1 with 0.6g, the drift ratio of the SD-C frame reached a higher value by 2.2 times the DRFT-C system shown in Fig. 8. As shown in Fig. 9 the drift ratios are well distributed for SCWB-C and DRFT-C frames at EQ2 0.3g. The drift ratios of the SD-C frame increased with the increase of the intensity of earthquake ground motions. The drift ratio of SD-C model showed about 10% radian under 0.6g in PGA shown in Figure 10. According to the result of the SD-C frame, the drift ratio increased with the increase of the peak ground acceleration(PGA). The primary reason for this high drift ratio at the upper floors was that the SD frame was designed only by the required strength without checking drift or strong column-weak beam conditions. In case of the other two frames, SCWB-C and DRFT-C frames, the drift ratio slightly increased. However, the overall shape of drift ratio plot showed twisted lines for in SCWB-C and DRFT-C frames shown in Fig. 10.

The drift ratios were well distributed over the stories in the case of the DRFT-C frame. On the other hand, the

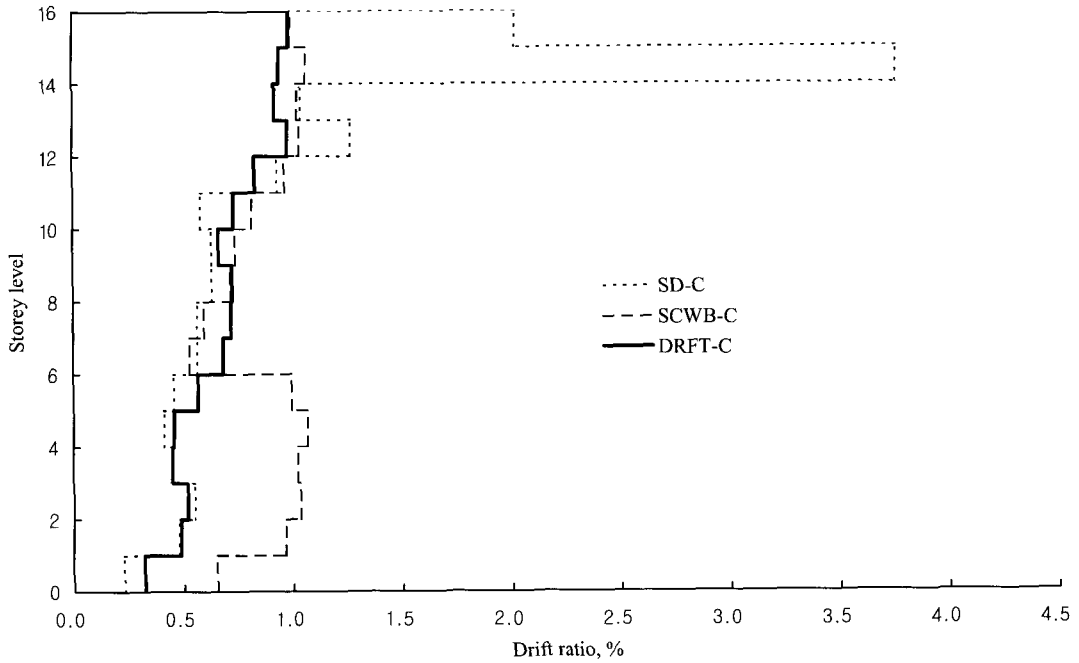

Fig. 7 Strength and stiffness effects by drift ratio at EQ1 0.3g

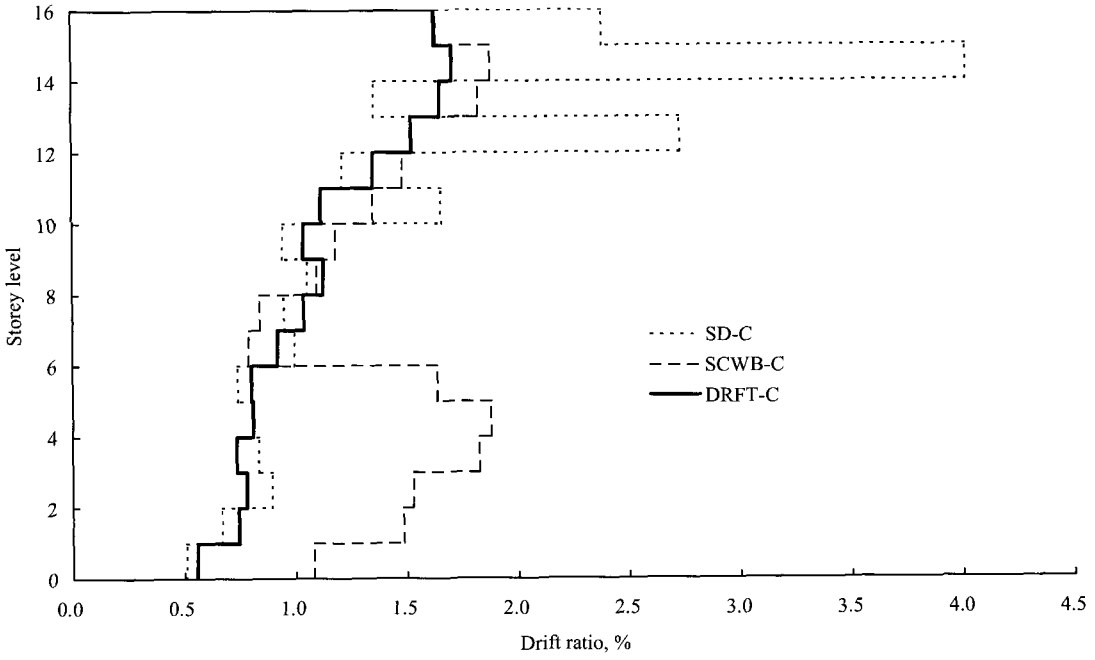

Fig. 8 Strength and stiffness effect explained by drift ratio at EQ1 0.6g

SCWB control model(SCWB-C) showed slightly higher drift ratios at the lower levels up to 4th floor compared with the one of DRFT-C model in all three earthquakes with 0.3g in PGA. Generally the drift ratio of the SCWB-C frame resulted in the similar drift ratios to the one of the DRFT-C frame at the seismic loadings up to 0.3g levels in PGA. If the earthquake ground motion increased up to 0.6g in PGA, the drift ratio of the SCWB-C frame increased by 43% and 100% compared with the DRFT-C frame at the 5th and 10th floors, shown in Fig. 10. However, the drift ratios of DRFT and SCWB models ranged from 1.0% to 3.5% point over all floors for all earthquakes in 0.6g. The drift responses of the SCWB-C and DRFT-C frames were similar to each other under the seismic loading of 0.3g in PGA. Accordingly, in the drift ratio results under the low seismic loading as much as 0.3g, the drift limitation by code did play a role in decreasing the drift ratio for the DRFT-C frame under the seismic loading of 0.3g for the steel moment resisting frames. However, this study shows that the drift ratio limitation by code is very crucial and beneficial for medium and high seismic areas having PGA beyond 0.3g.

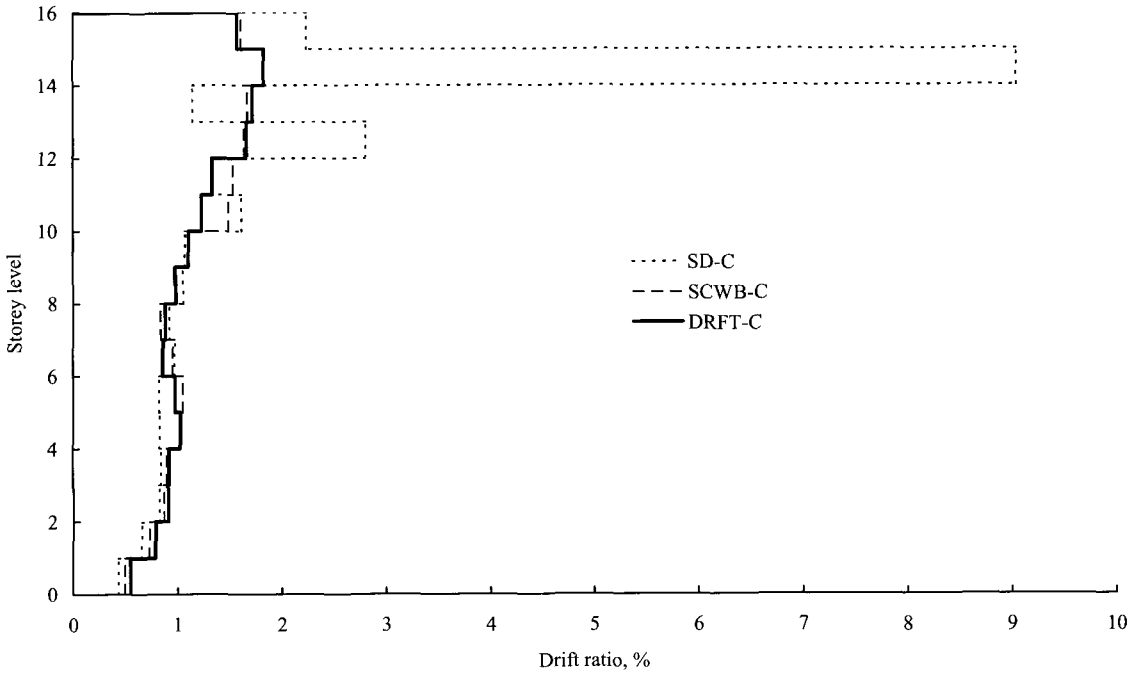

Fig. 9 Strength and stiffness increase effects explained by drift ratio at EQ2 0.3g

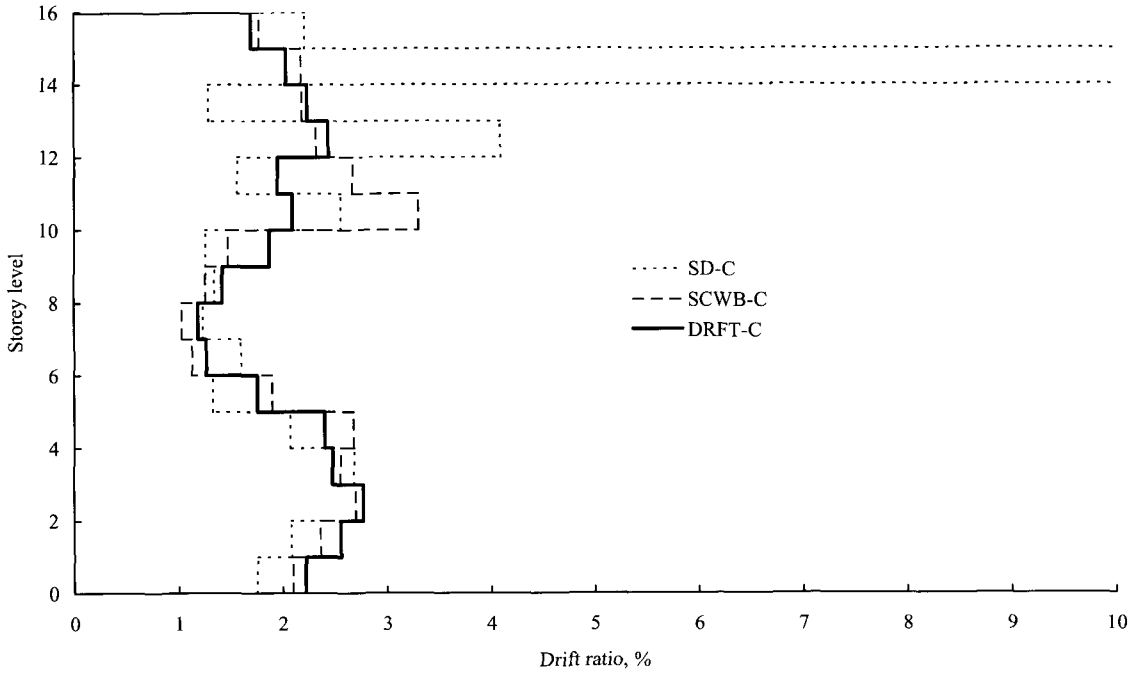

Fig. 10 Strength and stiffness increase effects explained by drift ratio at EQ2 0.6g

The plastic hinge rotations of the three basic systems are shown in Fig. 11 with EQ1 0.6g. The SD-C frame showed weak plastic rotation behavior compared with the other two frames under the increased seismic intensity. The high plastic hinge rotation distribution correlated with the higher drift ratio at the upper floors for the SD-C model. These high drift ratios also explain the results of hysteretic energy distribution. The weak strength effect clearly appeared in the results from EQ2 with 0.6g shown in Fig. 12. The overall plastic hinge resulted in values smaller than 0.1% radian at the lower seismic intensity like 0.3g for all frames. However, higher plastic rotation occurred in the SD-C frame.

As far as structures are designed by keeping one of regulations such as strong column-weak beam and drift limitation conditions, the drift ratio resulted in small values in this type of high-rise steel moment resisting frames. This was well represented by the results of the low plastic hinge rotations for SCWB-C and DRFT-C frames. However, if structures are designed only to satisfy strength requirements, it is unsafe for SD frames at high seismic intensity areas like SD-C frame and drift ratio can increase greatly in high seismic intensity areas beyond 0.3g in PGA, regardless of taking advantage of longer periods. Also, at high seismic intensity, the SCWB-C design can cause high drift ratios at the lower floors. Thus, it is important to keep strong column-weak beam conditions and drift limitations in designs at the seismic intensity regions.

5.3 Vertical mass irregularities

The vertical mass irregularity of sixteen story steel moment resisting frames was evaluated in this section. The three schedules of mass irregularities were studied. The mass variations were made artificially to investigate the seismic responses. The mass differences were 200% in an adjacent story of 2nd-floor, 8th-floor, and 15th-floor, respectively. The drift ratio and plastic rotation were discussed for the SD and DRFT systems with EQ1, EQ2, and EQ3. The strength and stiffness characteristics of the SCWB system showed a similar pattern to the DRFT system. Thus, the results of the SCWB system were omitted.

The drift ratio results were compared to the control system in Fig. 13 and Fig. 14 with 0.6g in the EQ2. In Case 1, the drift ratio was increased by 48% compared with the Control frame at the first floor for the SD system shown in Fig. 13. The drift ratio was also increased by 31% point compared with Control frame at the 8-floor at the Case 2. The drift ratio for the Case 3 was increase by 80% compared with the control system under EQ2 scaled to 0.6g in PGA. The drift ratio reached 4.87% in Case 3.

The drift response was evaluated for the DRFT systems with the vertical mass irregularities at the three places for three earthquakes at 0.3g and 0.6g. The drift ratio increased by 25% in Case 1 with EQ2, 0.6g shown in Fig. 14. The drift ratio increased slightly by 10% for the Case 2 under EQ2, 0.6g. The drift ratio increased by 117% in Case 3. To support the drift results, the plastic hinge patterns were plotted in Fig. 15 and Fig. 16. For the SD systems shown in Fig. 15, the large plastic hinges occurred at the upper floors in the Case 3. The plastic rotation results showed that the vertical mass irregularity of Case 2 was not significant while the other two cases showed large plastic rotation response under the EQ2, 0.6g. For the DRFT system shown in Fig. 16, the size of plastic rotations decreased due to the design characteristics which are apparent from the drift limit and strong column-weak beam conditions.[1] Generally, the plastic rotations increased at the upper floors

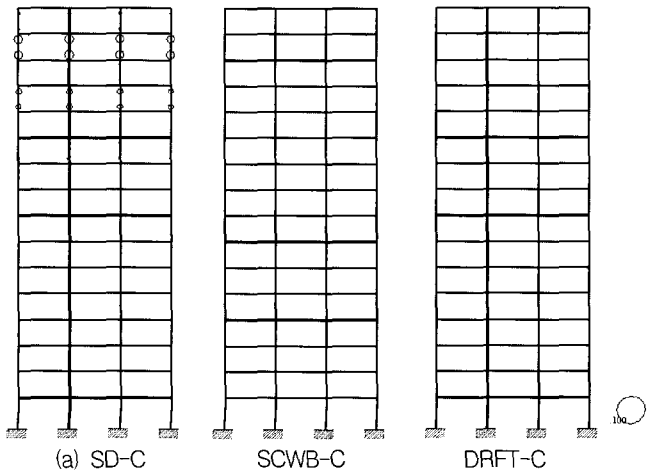

Fig. 11 Plastic rotations of three basic systems, EQ1 0.6g

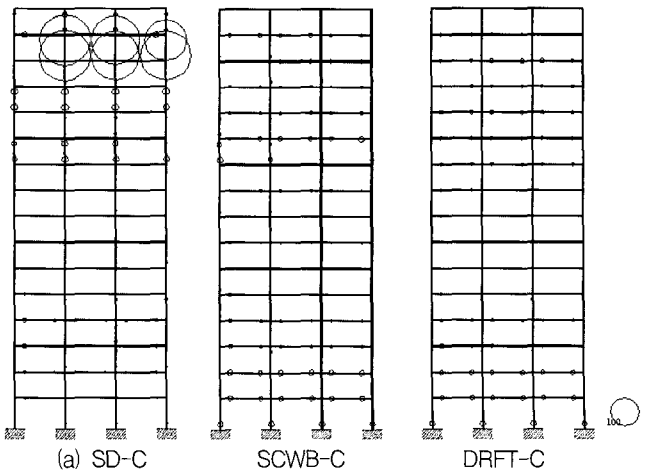

Fig. 12 Plastic rotations of three basic systems, EQ2 0.6g

in the Case 3.

The results showed that the drift ratio could increase significantly while plastic hinge rotations are not a major problem in the structure. The results also showed the drift ratio increment ranged from 10% to 117%. In all cases, the drift ratio increased where vertical mass irregularity has occurred in all cases. Among the three cases, the mass irregularity effect in Case 1 and Case 3 were more significant than Case 2 where the vertical mass irregularity was artificially made. The mass irregularity effect using the Case 2 was minor compared with the other two frames. The mass variation at the first floor and upper floors can cause serious drift ratio increment as shown in Case 1 and Case 3. The plastic hinge rotation distributions for the DRFT frame were not significant: about 1.0% radian for high-rise steel moment resisting frames. Also, plastic hinges tend to concentrate at areas where mass irregularities are made. If a mass(weight) irregularity exists in any story mentioned above, a drift ratio response is critical, rather than plastic hinge rotations for this type of high-rise steel

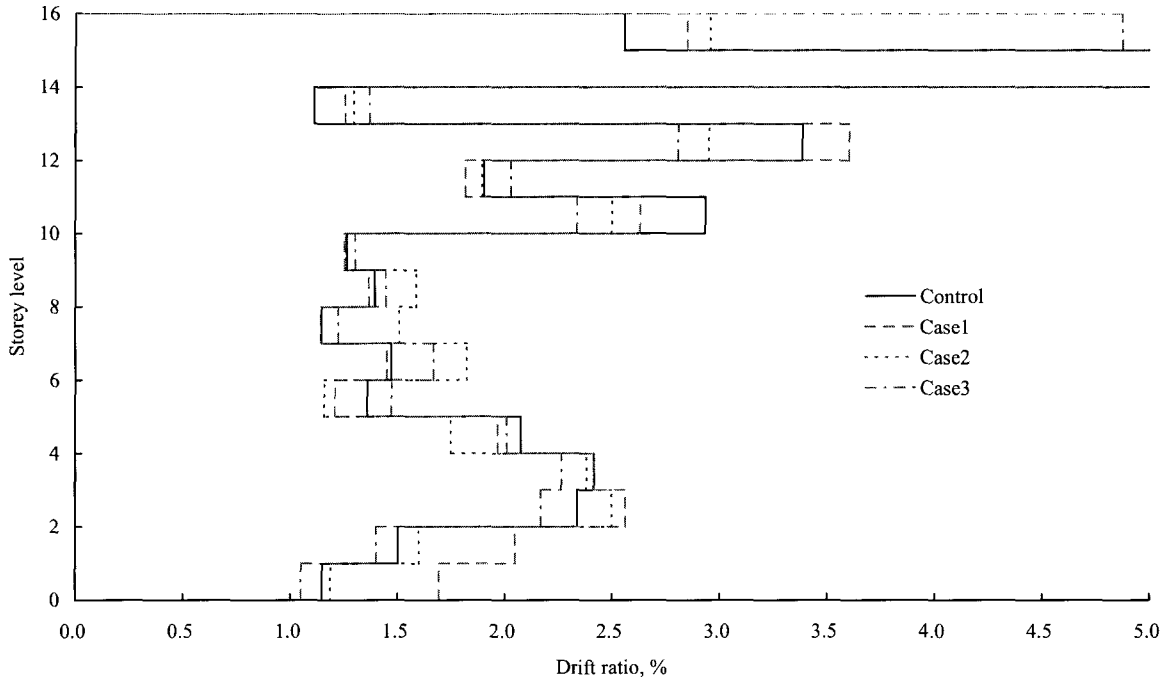

Fig. 13 Drift Ratios of SD frames with vertical mass irregularities, EQ2, 0.6g

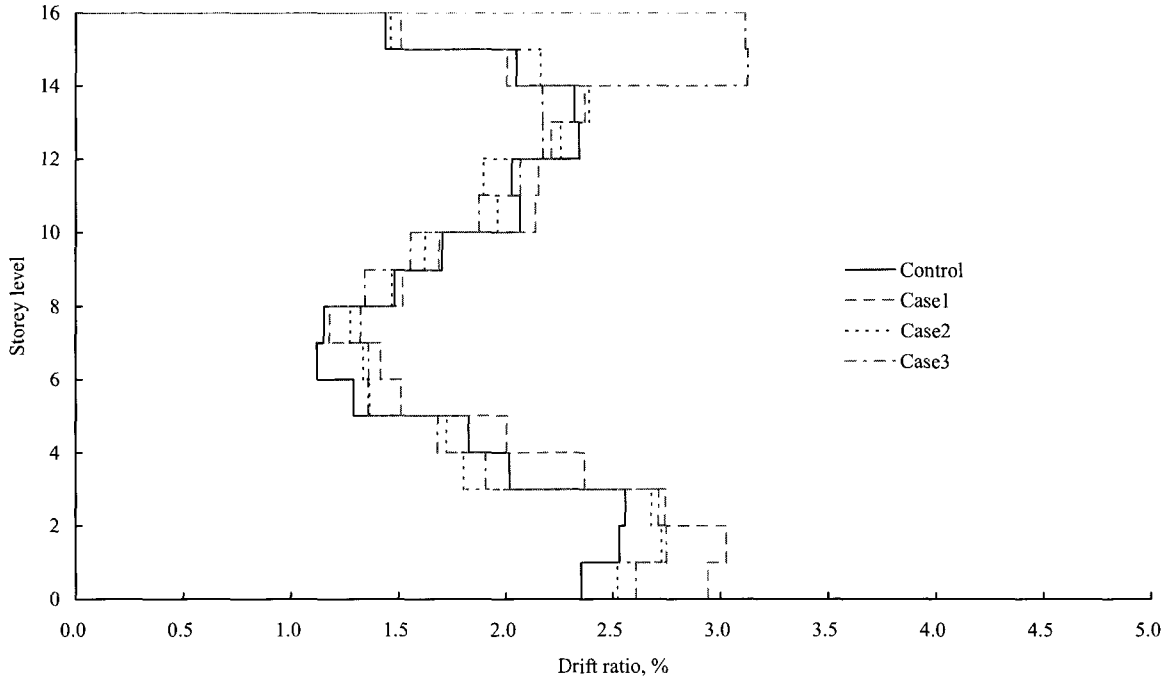

Fig. 14 Drift ratios of DRFT frames with vertical mass irregularities, EQ2, 0.6g

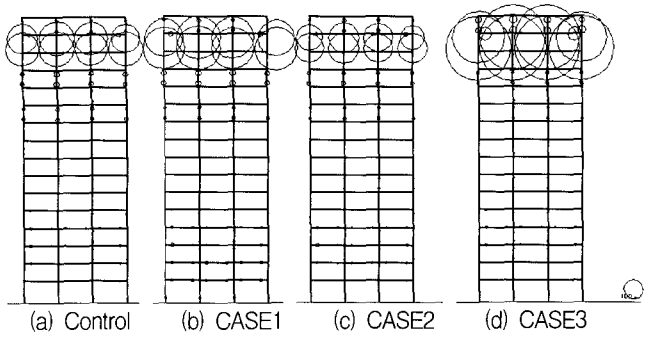

Fig. 15 Plastic rotations of SD systems with mass irregularities, EQ2, 0.6g

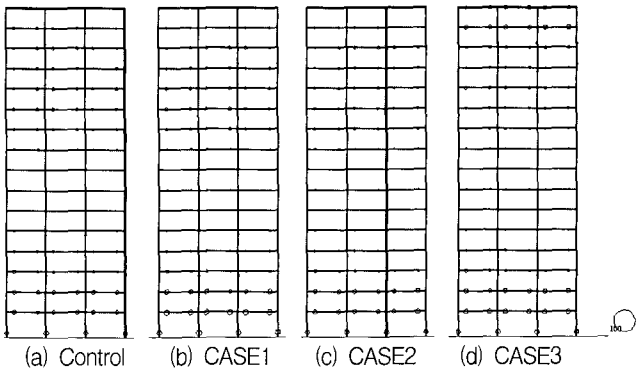

Fig. 16 Plastic rotations of DRFT systems with mass irregularities, EQ2, 0.6g

moment resisting frames.

If a mass irregularity more than 200% of an adjacent story exists, the drift ratio response is more important than the plastic rotation response. Thus, the research reassured that the drift ratio could reach more than 5% radian under the guideline value of 200% of vertical mass irregularity of UBC from the studied Case 3 model. The general drift ratios for DRFT frames were shown in Table 3.

Based on the provided drift response table 3, the average drift ratio of the Control frames was 1.55% under three earthquakes at 0.3g. The average drift ratio of the Control frames was 2.10% under three earthquakes at 0.6g. The results showed the most severe case of vertical mass irregularity was caused by the change in mass at the upper floors, as in Case 3. Then, the next severe case caused by mass variation at the lower stories, as in Case 1. The drift increase ratio in average was 28% and 199% at 0.3g and 0.6g, respectively in Case 3. The drift ratio for Case 1 increased up to 23% and 32% at 0.3g and 0.6g, respectively on average. Therefore, it is more dangerous if vertical mass irregularities occur at the lower or upper floors, than if they occur in the center levels of the structure.

5.4 Hysteretic energy input of systems

The hysteretic energy input results are shown in Fig. 17 and Fig. 18. The hysteretic energy inputs of the DRFT system are studied to identify the vertical mass irregularity at the EQ2 shown in Fig. 17. The hysteretic energy distribution showed a good distribution pattern over the height in the DRFT system. In Case 1 the hysteretic energy increased by 80% at the first floor. The hysteretic energy input increased by 51% in Case 2. Also, the hysteretic energy showed 46% increment in Case 3. As we have seen in Fig. 17, the greater increment of the hysteretic energy input demand occurred in the order of Case 3, Case 1, and Case 2, respectively.

The hysteretic energy input demands of the beams and columns are shown in Fig. 18. The figure considered as a reasonable output because the DRFT system was designed by observing the strong column-weak beam conditions of 1997 UBC. The hysteretic energy input demands on the beams at the upper floors were higher than the demands of the middle and lower floors. The similar hysteretic energy input patterns resulted in other earthquakes, too.

Overall hysteretic energy input demand of all frames were shown in Table 4 through 6. In the study, the hysteretic energy input demand of SCWB and DRFT frames was smaller than that of SD frames. The hysteretic energy input demand did not vary under the mass irregularity effect. However, we have to note that hysteretic energy input demand can increase without much variation of total hysteretic energy input demand at the certain floor where the vertical mass irregularity is created.

Until now the vertical mass irregularity effect has been studied with parameters such as drifts, plastic rotations,

Table 3 Maximum drift ratio and drift increase rate of the DRFT frames

PGA	Story	Maximum drift ratio(%) of Control				Drift increase rate(%)											
						Case1				Case2				Case3			
		EQ1	EQ2	EQ3	Avg.	EQ1	EQ2	EQ3	Avg.	EQ1	EQ2	EQ3	Avg.	EQ1	EQ2	EQ3	Avg.
0.3g	-	0.99	1.87	1.83	1.55	10.21	38.24	24.88	22.99	10.60	10.58	7.02	6.22	16.22	40.01	34.41	27.87
	Story	15~16	15~16	15~16	-	1~2	1~2	1~2	1~2	15~16	7~8	7~8	-	7~8	15~16	15~16	-
0.6g	-	2.56	2.77	2.77	2.10	46.54	26.4	23.78	31.79	13.81	19.16	15	12.28	451.49	116.39	36.69	198.84
	Story	14~15	2~3	2~3	-	1~2	1~2	1~2	1~2	3~4	6~7	6~7	-	1~2	15~16	15~16	-

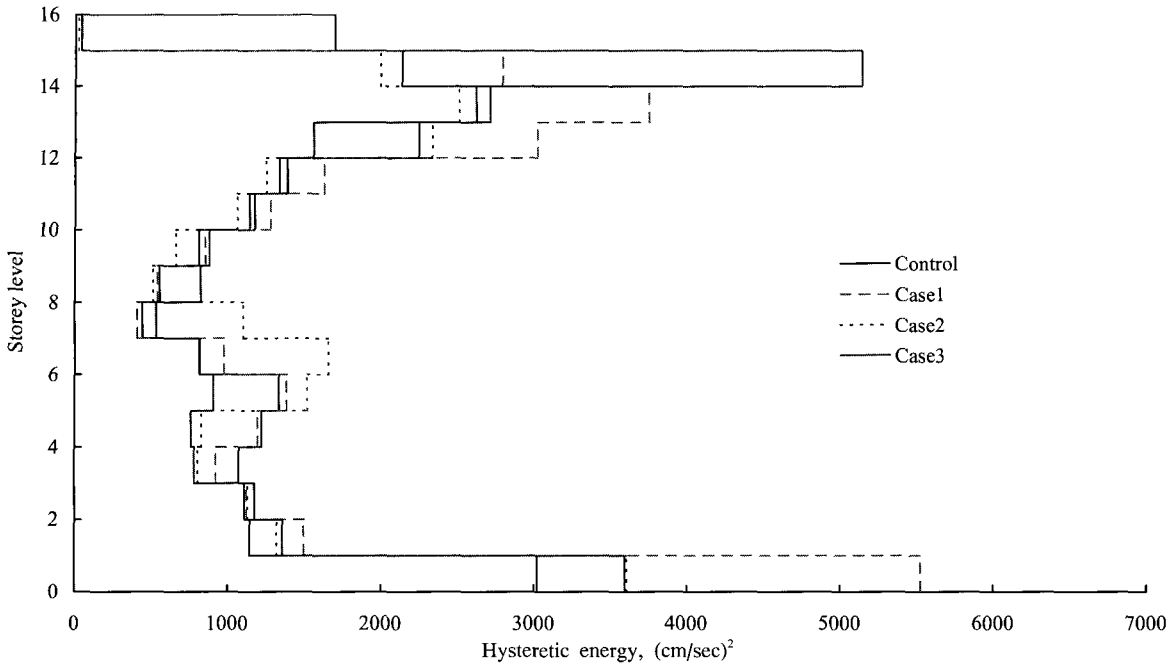

Fig. 17 Hysteretic energy inputs with mass irregularity effects of DRFT frames, EQ2, 0.6g

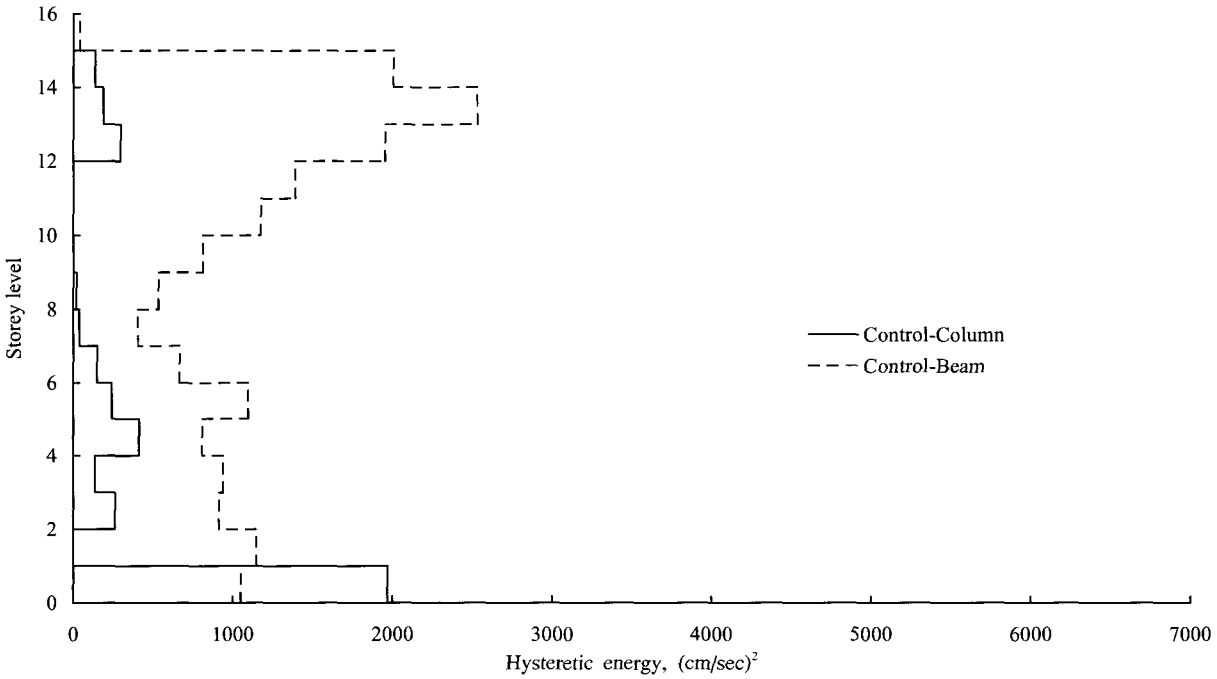

Fig. 18 Hysteretic energy input of beams and columns with mass irregularity of DRFT frame, EQ2, 0.6g

Table 4 Normalized hysteretic energy input of SD frames(m=3.5469 tf-s²/cm)

Cases	Control Frame		Case 1		Case 2		Case 3	
PGA	0.3g	0.6g	0.3g	0.6g	0.3g	0.6g	0.3g	0.6g
EQ1	170	1063	243	2266	175	1842	206	1952
EQ2	1052	7341	3072	9276	1275	8145	1226	8130
EQ3	652	7010	945	4519	720	4043	733	4070
Average	625	5318	1420	5354	723	4676	722	4717

and input energies. The stress response at the beam-column connection was included in this essay to explain the stress demand using finite element analysis. To examine the stress demand for Case 1, DRFT-C frame, the same condition of load and vertical mass irregularity were used to simulate the mass irregularity effects. The same member sizes of

DRFT-C frame at the first floor were used. The two dimensional plate elements were used to make simple model. The stress demand of the beam-column connection was shown in Fig. 19. The maximum stress near the connection area was about 96kgf/cm^2 with EQ 3, 0.6g. The minimum stress was about 7.2kgf/cm^2 for the DRFT-C frame. The stress demand showed that the maximum stress occurred in the top flange of the beam and propagated into the panel zone. In that case the stress demand at the lower flange of the beam and panel zone was minor.

The damages were formed widely from the connection area to the panel zone. The damage at the middle part of the beam was not significant. The simulated stress results showed that the damage mainly occurred at the upper beam flange and upper panel zone. Then, the energy demand propagated to the lower flange of the beam column connection areas.

Finally an empirical curve of the hysteretic energy input demand is presented in Fig. 20. This curve is well accorded in the results of former researcher.[17] In Fig. 20, the hysteretic energy input was illuminated by the variation of natural period by adding current results to the ones of Choi and Shen. The empirical equation can be drawn using interpolation from the results:

$E_h/m = -2092 \cdot \ln(T) + 3332$
$0.5 \le T < 5.0$ and $PGA \le 0.3g$
$E_h/m = -8334 \cdot \ln(T) + 15865$
$0.5 \le T < 5.0$ and $0.3g < PGA \le 0.6g$

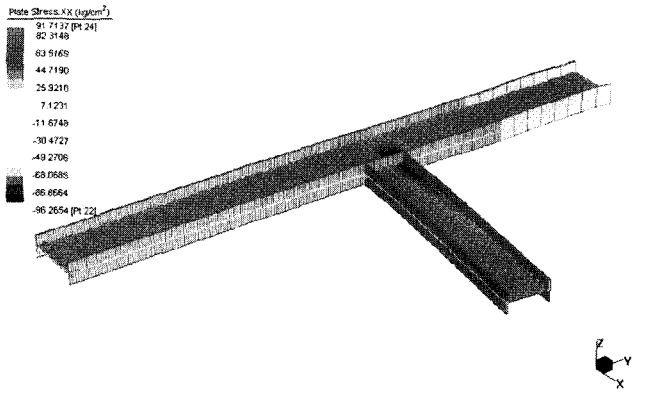

Fig. 19 Stress demand at 1st floor of DRFT frame for Case 1, EQ 3 0.6g

Here E_h/m is the normalized hysteretic energy input demand and T is the target period of structures. The results have two important implications. First, the hysteretic energy of systems decreases with increasing period. In the same fashion, the hysteretic energy of structures increases with increasing base shear coefficient(V/W). Secondly, the mean hysteretic energy input of MDOF systems can be approximated from Fig. 20. All of the hysteretic energy input results are tabulated in Table 4, 5, and 6.

The presented curve represented that hysteretic energy input demand gradually decreased with the increase of the natural period of vibration. The empirical equation was valid only in limited regions. The hysteretic energy input demand can be estimated with a known T. Therefore, the empirical curve of the energy input demand is valuable as a design tool that uses an energy approach for steel moment resisting frames.

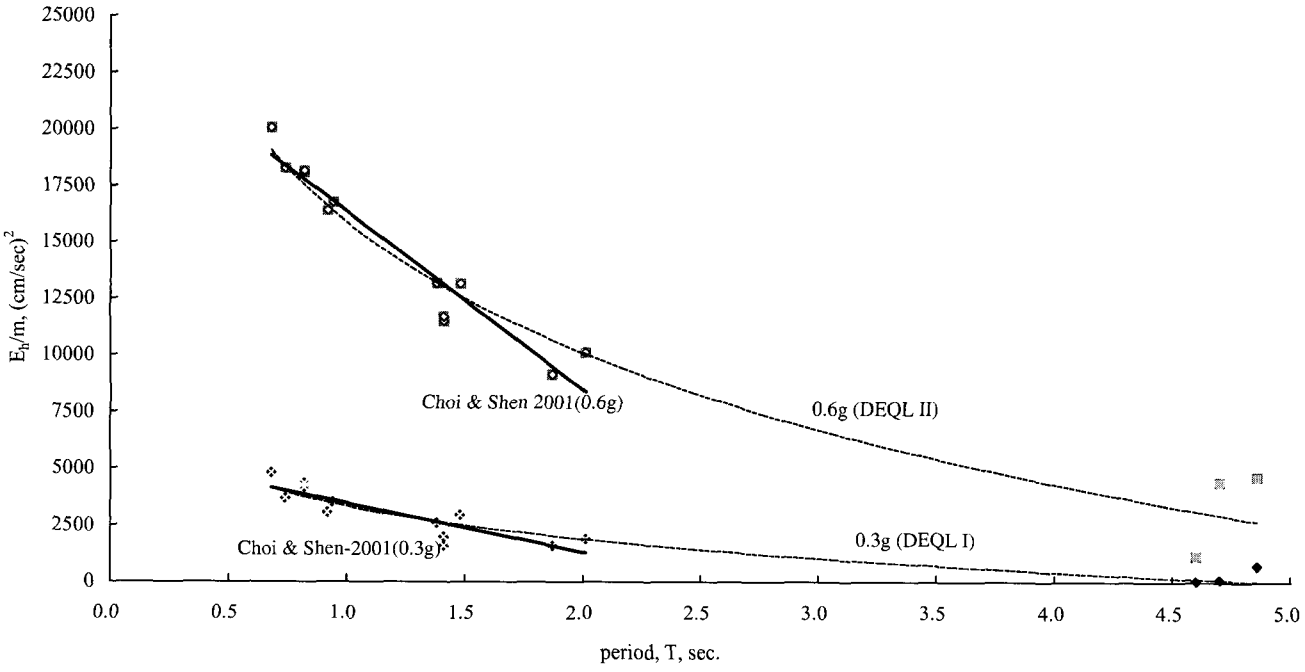

Fig. 20 Revised empirical hysteretic energy normalized by mass of steel moment resisting frames

Table 4 Normalized hysteretic energy input of SD frames(m=3.5469 tf-s²/cm)

Cases	Control Frame		Case 1		Case 2		Case 3	
PGA	0.3g	0.6g	0.3g	0.6g	0.3g	0.6g	0.3g	0.6g
EQ1	170	1063	243	2266	175	1842	206	1952
EQ2	1052	7341	3072	9276	1275	8145	1226	8130
EQ3	652	7010	945	4519	720	4043	733	4070
Average	625	5318	1420	5354	723	4676	722	4717

Table 5 Normalized hysteretic energy input of SCWB frames(m=3.5469 tf-s²/cm)

Cases	SCWB Control		Case 1		Case 2		Case 3	
PGA	0.3g	0.6g	0.3g	0.6g	0.3g	0.6g	0.3g	0.6g
EQ1	0	967	4	1374	2	1086	5	1062
EQ2	264	6552	427	8038	261	6933	2493	7374
EQ3	652	3524	436	3807	243	3375	335	3450
Average	305	3681	289	4407	169	3798	944	3962

Table 6 Normalized hysteretic energy input of DRFT frames(m=3.5469 tf-s²/cm)

Cases	DRFT Control		Case 1		Case 2		Case 3	
PGA	0.3g	0.6g	0.3g	0.6g	0.3g	0.6g	0.3g	0.6g
EQ1	9	976	11	1386	33	1386	5	1079
EQ2	259	6336	233	6010	384	7605	228	6302
EQ3	386	3634	353	3430	490	3794	305	3399
Average	218	3649	199	3609	295	4262	179	3593

6. Conclusions

Mass irregularity is one of the important factors affecting structural responses under seismic loadings. This paper presented the seismic responses of structures with the vertical mass irregularities using high-rise steel moment-resisting frames. The drift ratio, plastic rotation, energy distribution, and stress in element level were investigated. Based on the research, the following conclusions can be drawn.

The more a structure is strengthened and stiffened, the less the drift ratio will occur. As far as structures are designed by keeping one of the regulations such as strong column-weak beam and drift limitation in the high-rise steel moment-resisting frames, the plastic hinge and drift ratios are of small values in seismic intensity up to 0.3g in PGA. However, with structures that are designed with both strength and strong column-weak beam requirements, (SD and SCWB frames in the study), high drift ratios with increased seismic intensity like 0.6g in PGA occur. Accordingly, the observed drift ratio of UBC-97 or similar code in design is much more meaningful in high seismic regions.

From the investigations of the vertical mass irregularities, the average drift ratio of the Control frames was 1.55% and 2.10% under three earthquakes at 0.3g and 0.6g, respectively. The results showed the most severe case of vertical mass irregularity was to change the mass at the upper floors as in Case 3. Then, the next severe case was to change mass at the lower stories as in Case 1. The drift increase ratio on average was 28% and 199% at 0.3g and 0.6g, respectively in Case 3. The drift ratio for Case 1 increased up to 23% and 32% at 0.3g and 0.6g, respectively on average. Therefore, it is dangerous if vertical mass irregularities occur at the lower or upper floors rather than at the center of the structure. The plastic hinge rotations and energy distribution well supported the statements.

The hysteretic energy input demands were increased at a higher rate than the one of the drift ratios. For instance, the hysteretic energy of 80% was increased by the vertical mass irregularity of the first floor, Case 1. The hysteretic energy input demands were increased by 51% and 46% at the middle and the roof floors where the vertical mass irregularities were made. As far as the structure is designed in satisfaction of the strong column-weak beam condition, larger hysteretic energy demand occurred in the beams than the columns, except with the first floors. Thus, careful attention is needed to avoid weak story mechanism in a structure. Based on this study's results, the hysteretic energy input demand curve was acquired in a relationship between hysteretic energy input and natural period at 0.3g

and 0.6g in peak ground accelerations. This proposed curve was acquired empirically by the compiling of various multi-degrees of freedom systems. Thus, an empirical curve of the hysteretic energy input demands could be used for the energy designs and applications.

Even though the hysteretic energy study has been carried, there still exists many unknowns. In the future, the vertical mass irregularity needs to be compared in various structural systems such as braced frames and shear wall frames. Future studies may include other structural systems and more seismic records to provide more appropriate information about the hysteretic energy input of the regular and irregular structures.

Notation

A_g : Gross area of a column, cm^2
F_{yb} : Specified minimum yield strength of a beam, kgf/cm^2
F_{yc} : Specified minimum yield strength of a column, kgf/cm^2
H : Average of the story heights above and below the joint, cm
P_{uc} : Required axial strength in the column (in compression) ≥ 0
V_n : Nominal strength of the panel zone,
Z_b : Plastic section modulus of a beam, cm^3
Z_c : Plastic section modulus of column, cm^3
d_b : average overall depth of beams framing into the connection, cm.

Acknowledgements

This work was supported by the Korea Research Foundation Grant(KRF-2002-003-D00407).

References

1. UBC-Uniform Building Code, *International Conference of Building Officials*, Whitter, California, 1997.
2. FEMA 274, *NEHRP Commentary on the Guidelines for the Seismic Rehabilitation of Buildings*, FEMA, 1997, pp. 5-10.
3. Uang C-M. et al., "Seismic response of an instrumented 13-story steel frame building damaged in the 1994 Northridge earthquake," *Earthquake Spectra*, Vol. 13, No. 1, 1997, pp. 131-148.
4. Kuwamura, H. and Galambos, T. V., "Earthquake load for structural reliability," *J. of Structural Engrg.*, ASCE, Vol. 115, No. 6, 1989.
5. Akiyama, H., *Earthquake-resistant Limit State Design for Buildings*, Univ. of Tokyo Press, 1985.
6. Valmudnsson, E. V. and Nau, J. M., "Seismic response of building frames with vertical structural irregularities," *J. of Structural Engrg.*, Vol. 123, No. 1, 1997, pp. 30-41.
7. Chopra, A. K., *Dynamics of Structures - Theory and Applications to Earthquake Engineering*, Prentice Hall, 1995, pp. 264-265.
8. Mahin, S. A. and Bertero, V. V., "An evaluation of inelastic seismic design spectra," *J. of Structural Div.*, ASCE. Vol. 107, No. 9, 1981.
9. Uang, C-M and Bertero, V. V., "Evaluation of seismic energy in structures," *Earthquake Engrg. and Structural Dynamics*, 1990, pp. 77-90.
10. Fajfar, P. et al., "On the energy input in the structures," *Pacific Conference on Earthquake Engrg.*, New Zealand, 1991, pp. 81-92.
11. Nigam, N. C. and Jennings, P. C., *SPCEQ/UQ, California Institute of Technology*, CA, June 1968.
12. Tsai, K. C. and Li, J. W., DRAIN2D+ *A General Purpose Computer Program for Static and Dynamic Analyses of Inelastic 2D Structures Supplemented with a Graphic Processor*, Report No. CEER/R83-03, Center for Earthquake Engrg. Research, National Taiwan Univ., 1994.
13. Strand7, *G+D Computing*, Sydney, Australia, 2002.
14. Zarah, T. F. and Hall, W. J., "Earthquake energy absorption in SDOF structures," *J. of Structural Engrg.*, ASCE, Vol. 110, No. 8, 1984, pp. 1757-1772.
15. Leger, P. and Dussault, S., "Seismic energy dissipation in MDOF structures," *J. of Structural Engrg.*, ASCE, Vol. 115, No. 9, 1992.
16. LRFD, *Manual of Steel Construction Load & Resistance Factor Design*, Volume I, Second Edition, LRFD-AISC, 1995.
17. Choi, B. J. and Shen, J. H., "Empirical hysteretic energy with strength, strength and drift, and SCWB designs using steel moment resisting frames," *The Structural Design of Tall Buildings*, Vol. 10, No. 1, 2001.